11.5 Modules

11.5.1 Introduction and Effect of Environment

A module is the basic functional sub-unit of the ATLAS SCT. It consists of a set of single sided silicon micro-strip detectors glued back to back, an electronics package (the "hybrid") and an interface to the cooling and mechanical support structure of the tracker. There is a single module design for the SCT barrel region, and three designs for the various radial locations in the SCT forward regions. A number of electrical, thermal, and mechanical requirements constrain the design of the SCT modules. This section of the SCT TDR addresses the design and performance of the modules. Chapter 11.10 will address separately the process by which large numbers of modules will be constructed for the SCT.

In the present sub-section the effect of the SCT and LHC operating environment on the design of modules for the SCT is discussed. Section 11.5.2 details the actual specifications on the module design. In Section 11.5.3 the module design is described. In Section 11.5.4 the expected performance of the modules is discussed together with prototype results. Finally, a materials compilation is given in Section 11.5.5.

There are four main issues which arise from the requirements of the SCT and LHC operating environment and affect significantly the design of the module. The first issue concerns the general event topology at the LHC and affects the division of the tracker into a barrel and forward region. The second issue concerns tracking performance and translates into constraints on the mechanical precision and stability of the module and its electrical performance. The third issue concerns radiation levels and the thermal design of the module. This is because radiation effects are strongly temperature dependent. The fourth issue concerns the effect of material within the module on the performance of the tracker and the other outside elements of the ATLAS detector. This leads to serious constraints on materials to be used in the construction of the modules.

11.5.1.1 Event topology

For the event configurations at LHC, the requirements of rapidity coverage ($|\eta|<2.5$) and an effective use of silicon area lead naturally to a division of the tracker into a central barrel region and a forward disk region. Effective overlap along z and a minimization of dead regions leads to a barrel module configuration with the hybrid electronics package mounted over the active region of the silicon, rather than off the end as was common in small vertex detectors. The physical limitations of available silicon leads to a barrel module length of 12.8 cm. In the forward region, the natural disk geometry and a restriction of the length of a module to around 12 cm or less leads to the concept of using three rings of detectors to provide the necessary radial coverage. The forward modules are supported at the outer end which is then the natural location of the hybrid.

11.5.1.2 Tracking

The precision that will be achieved is determined by the readout pitch of the strip detectors, by the assembly and survey precision of the module, and by the tilt angle and mounting and survey precision of the module on the support structure. The first two factors are considered here.

The tilt angle is discussed as part of the overall layout of the SCT in Section 11.2.2. The mounting precision is discussed in Section 11.8 and Section 11.11 which concern the mechanical support structure and assembly of the SCT.

For the SCT barrel, the required tracking precision is obtained by modules with an intrinsic point resolution of 23 μm in the r-ϕ coordinate per single side measurement. The precision is obtained for the binary readout scheme discussed in Section 11.4 using detectors with 80 μm readout pitch. A back-to-back detector pair with a stereo rotation angle of 40 mrad gives a precision of 17 μm in the r-ϕ coordinate and 500 μm in the z coordinate from the correlations obtained through fitting. To maintain these resolutions high quality module construction, metrology, and subsequent position monitoring is required. The mechanical tolerance for positioning wafers within the back-to-back pair must be ~ 5 μm in lateral strip position, 25 μm in module thickness, and 25 μm in z.

The forward region measures the longitudinal momentum and the track dip angle. The requirements are very similar to the barrel after allowing for interchange of r and z.

For pattern recognition, noise occupancy must be kept low. Electronic noise analyses for the shaping times used in SCT show that a centre tapped configuration will have the minimum noise contribution from the series resistance of the readout strip. The improvement over an end tapped configuration is about 150 electrons [11-68].

Within the SCT structure the barrel modules are intrinsically suitable to benefit from the centre-tap scheme, while in the forward region other considerations become relevant. In particular, the radial dependence of the background radiation enhances the need to place active electronic components at the largest possible radii, and hence makes an end-tap readout more attractive. The natural cooling structure for forward modules also shows some advantages for this configuration.

After considering the combined electrical, thermal and mechanical requirements the optimised modules will use centre-tap hybrid readout in the barrel region and end-tap for the forward region. Both the geometry and components of these modules are detailed in Section 11.5.3.

11.5.1.3 Radiation level

The severity and consequences of the high accumulated radiation levels for silicon detector operation are considered in Section 11.3.1. A result of the increased leakage current and the type inversion is the need to operate detectors at -7°C. The maximum expected fluence after 10 years of operation in the SCT is 2.15×10^{14} n/cm^2 (including a 50% safety margin). This will result in a total leakage current of ~ 1.3 mA for a module operated at -7°C. The corresponding depletion voltage will be in the range 300-400 volts depending upon warm-up scenarios. As the modules are built at room temperature, and then cooled to -7°C, care must be taken to use material combinations which minimize thermal distortions.

Thermal considerations, and especially concerns of thermal run-away, lead to a module design where the effective in-plane thermal conductivity must be increased beyond that of silicon. In practice this will be achieved by the use of thermal heat spreading materials which are laminated as part of the detector sandwich.

11.5.1.4 Material

The need to minimise material puts additional constraints on the module design. Interactions will complicate the pattern recognition and track reconstruction, especially within jets. The energy measurement resolution of the Liquid Argon electromagnetic calorimeter will be degraded by material, as will the increased level of photon conversions.

11.5.2 Specification

In this sub-section specifications on the design of the SCT module are provided.

11.5.2.1 Mechanical configuration

In the barrel region, one module is made of four 6.4 cm x 6.36 cm single-sided silicon microstrip detectors. Geometrical dimensions are shown in Figure 11-50 for two detectors butt joined to form a 12.8 cm long mechanical unit. Strips of two of the detectors are electrically connected to form 12.6 cm long active strips. The detectors will be positioned to have a 2 mm gap at their join. In order to form a double-sided readout module, two 12.8 cm long mechanical units are back-to-back aligned and glued with a stereo angle of 40 mrad. One side of the module measures the r-ϕ coordinates ("axial strips") while the other side measures the 40 mrad rotated coordinate (the "stereo strips"). The pitch of the strips is 80 µm and there are 768 readout strips.

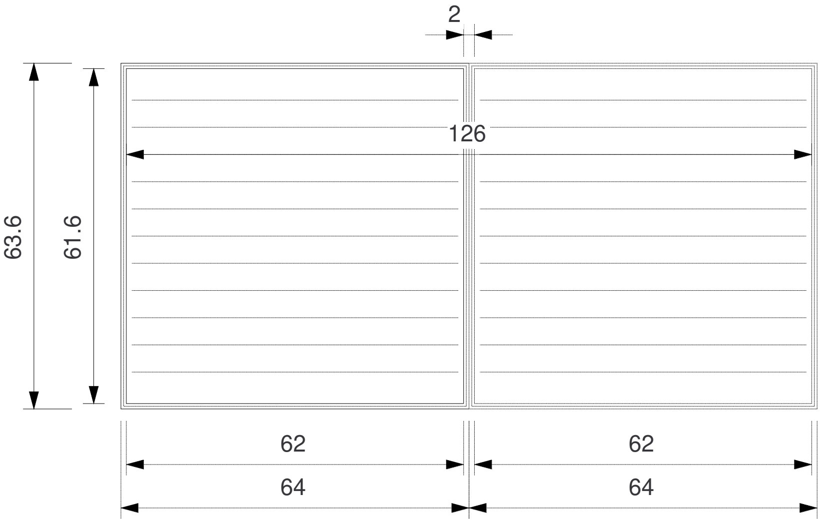

Figure 11-50 Geometry of barrel module detectors and configuration.

Initially the backside of the detector forms the *p-n* junction. When the detectors are glued back-to-back, the gap between the *p*-implant and the cutting edge must be sufficiently far from the glue line to prevent any electrical degradation.

In the forward region, each module is formed from two measuring planes. In the first plane, the azimuthal angle, ϕ, is measured directly via strips of a radial geometry in which the strip pitch varies along the module length. The second measuring plane, identical to the ϕ plane, is mounted such that there is a 40 mrad rotation with respect to the ϕ plane. The second plane provides a measure of the radial position of a particle when used in conjunction with the ϕ plane.

There are 770 strips per measuring plane, with the first and last being used for field shaping and not connected to the readout. Each module subtends an angle larger than that required, to allow for a reasonable number of overlapping strips to ensure hermiticity and to facilitate module-to-module alignment using physics tracks. The nominal ϕ angle of a module is covered by strips 10 to 759 where strips 0 and 770 are the field shaping strips. Figure 11-51 shows a schematic of the wafer dimensions and relative positioning for each of the three module types used in the forward region. Each wheel is covered by one to three rings depending on its z position in the tracker.

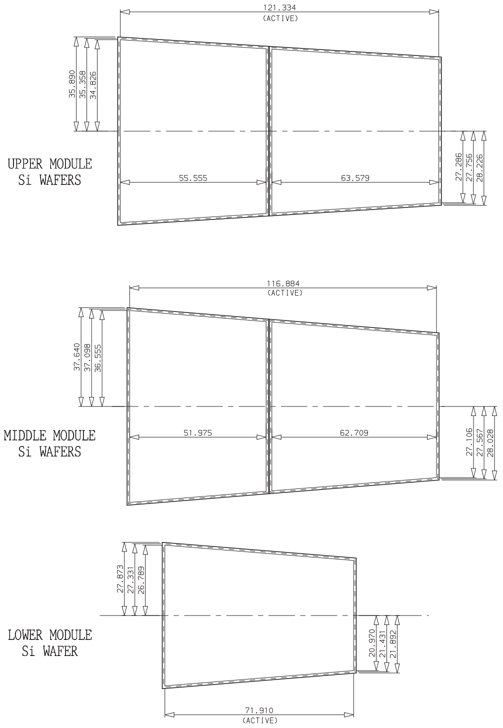

Figure 11-51 Geometry of forward silicon detectors.

The outer ring is covered by 52 modules and has an active strip length of 121.1 mm formed from two wafers butted end-to-end. The outer ring module subtends an angle of 7.117 degrees to allow for overlaps. The rotation point for the u/v stereo plane is at the intersection of the wafer break and the module centre-line.

The middle ring, covered by 40 modules is, with the exception of those modules on wheel 8, also formed from two butt-joined wafers and has an active length of 116.7 mm. The middle ring modules on wheel 8 are formed from the upper wafer only and consequently have an active length of 52 mm. Middle ring modules subtend an angle of 9.252 degrees and the rotation point for the U/V plane is at the intersection of the wafer break and the module centre-line.

The inner ring is covered by 40 modules, each having an active strip length of 72 mm formed from a single wafer, subtending an angle of 9.252 degrees. The rotation point for the U/V plane is at the intersection of the mid-point of the active length of the wafer and the module centre-line.

11.5.2.2 Mechanical tolerances

In the barrel, the strips on each of four detectors within a module should be relatively aligned to within ±5 μm in the ϕ direction and 25 μm in the z direction. The detector positions will be referenced to the overall support structure with dowel pins. The discussion of module placement accuracy upon the support structure is in Section 11.8. The overall error in strip position is a combination of the error in placement of the rigid four detector unit with respect to the dowel pins and the error in placement of the module upon the support structure. The rigid four detector unit is to be placed within 50 μm in the r-ϕ direction and 100 μm in the z direction relative to the dowel reference frame but surveyed to 5 μm. The discussion in Section 11.8 indicates that the radial location of a wafer needs to be known to 50 μm upon the support structure. The thickness and shape of the individual modules should therefore vary by less than 25 μm. The skew of the detectors relative to the dowel pin reference frame is such that one end of a 12.6 cm strip is within 100 μm of the other end of the strip. In the forward modules the specifications are the same except that the z direction of the barrel module is replaced by the r direction.

Table 11-21 Mechanical tolerances of the barrel module

	ϕ [μm]	r [μm]	z [μm]
Back-to-back pair	5	25	25
Strips to dowel pin	50	50	100
Stability	5	50	100
Module skew < 0.8 mrad			

11.5.2.3 Power consumption

The power consumption of the CAFE-M chip is 1.9 mW/channel and that of the ABC chip is close to 1 mW/channel (including the LVDS drivers which are used to transmit the data from the front end electronics to the off detector electronics). The total power dissipated by the hybrids on a module with 12 ABC and 12 CAFE chips will be 4.45 W. The thermal design of the module must allow for this.

11.5.2.4 Hybrid specification

Electrical aspects of the hybrid are discussed in Section 11.4.5. Some of the electrical specifications on the hybrid originate from the need not to electrically degrade the performance of the module. In addition, the hybrid is part of the mechanical and thermal linkage between the silicon detectors and the support and cooling systems. The module base-board contains the mechanical reference points (dowel holes) which link the strips to the support. These holes must be shaped and sized appropriately. The hybrid must be of a stiff and stable material. The hybrid must have sufficient thermal conductivity to allow most of the heat generated by the front end chips to be removed by the coolant. The hybrid must support the front end chips sufficiently to allow reliable wire-bonding to the detectors.

11.5.2.5 Operation temperature

As discussed in Section 11.5.1.3, the average operating temperature of the silicon detectors will be -7°C. This value has been chosen to ensure the minimum depletion voltage after irradiation. In addition, variation of the temperature over the detectors should be less than 5°C to maintain uniformity in the leakage current and the depletion voltage.

11.5.2.6 Thermo-mechanical distortion

The SCT will undergo temperature cycling over the range -15°C to +25°C in a controlled sequence, and it must be safe, in the event of cooling or local power fluctuations, at temperatures up to 50°C. This requires the module design to have minimal CTE, and to be capable of elastic deformation. The precision of the tracking measurement depends on the modules having a stable profile after changes of the operating conditions. To prevent fracture, permanent deformations should be $< 5\ \mu m$, and elastic deformations occurring across the full temperature range should be $< 50\ \mu m$.

11.5.2.7 Material

The material budgets for the barrel and forward modules are 1.20% and 1.28% of a radiation length respectively, when averaged over the full module area. Details are provided in Section 11.5.5.

The mechanical specifications are summarized in Table 11-22 and Table 11-23.

11.5.3 Description of module design

11.5.3.1 The barrel module

Figure 11-52 is a schematic of the barrel module showing the key features in the design. Figure 11-53 shows an expanded view of all the components. The measuring planes, each formed of a pair of wafers, are glued to a central beryllia baseboard and a pyrolytic graphite (TPG) heat spreader. The composite baseboard serves as a mechanical support for the wafers and increases the thermal conductivity in the plane of the module. Beryllia has been chosen for the hybrid base-board frame due to its mechanical rigidity, its high thermal conductivity (280 W/mK) and long radiation length. The TPG, with a thermal conductivity of 1100 W/mK, significantly increases the in-plane thermal conductivity of the module. As shown in the figure, the baseboard protrudes out symmetrically on both sides of the module. The exposed tabs are the points at which the readout hybrids attach to the module. The beryllia hybrids form mechanical bridges across the silicon, in a design that reduces the thermal coupling between the front end chips and the silicon without contacting the silicon surface. An effort has been made to avoid gluing to the active surface, given the uncertainties associated with long term ageing and radiation effects.

The cooling contact to the barrel module is made at one side as indicated in the diagrams. The contact point includes dowel pin holes to accurately locate the module on the support structure.

Table 11-22 Barrel module specification

Detector outer dimension	**63.6 mm x 128 mm**
Construction	Use four 63.6 mm x 64 mm *n*-on-*n* single sided detectors to form 128 mm long and back-to-back glued detectors
Mechanical tolerance	back-to-back: <5 µm (ϕ), <25 µm (r), <25 µm (z) Fixation point: <50 µm (ϕ), <100 µm (z)
Strip length	126 mm (2 mm dead in the middle)
Strip directions	Axial (along z-coordinate), U/V (40 mrad stereo)
Number of readout strips	768 per side, 1536 total
Strip pitch	80 µm
Hybrid	74.6 mm x 28 mm x 0.38 mm two single-sided hybrids bridged over the detector
Detector power consumption	1 W /total @ 0°C, (Heat flux/300 µm) ~ 70 µW/mm^2
Hybrid power consumption	4.45 W
Operating temp. of detector	-7°C (average)
Uniformity of silicon temp.	<5°C
Permanent deformation	<5 µm (after 10 thermal cycles between -20 and +70°C)
Power on-off (Detector & Hybrid)	<10 µm
Dynamical deformation	<50 µm (between -10 and +30°C)

An example of a prototype barrel hybrid is shown in Figure 11-54. They are single sided, multilayer thick-film circuits, fabricated on a cast or mechanically ground and laser profiled, with a beryllium oxide ceramic substrate. The width of the hybrid substrate is 74.6 mm. In the region of the support tabs they are 0.881 mm thick but in the central region they are 0.381 mm thick. The applied thick film layers add another 0.250 mm to the thickness. These hybrids will be produced using a thick film process specially developed for this application. This, together with the use of 50% gridded power planes, reduces the total radiation length of the metal layers by a factor of four as compared to a standard thick film process. Each barrel module will have two hybrids, one per side. Each hybrid will have six sets of CAFE-M and ABC readout chip pairs, mounted and aluminium wire bonded and a small number of passive de-coupling components which are attached by soldering. One hybrid will have a short "pig-tail" cable to connect the module to the outside. The two sides will be interconnected with a short "jumper" cable.

The hybrid circuit has five 3 µm thick screen printed gold interconnect layers on each side, with screen printed 200 µm vias and insulator layers (2*20 µm) between each interconnect layer. The first three metal layers on each side (nearest the substrate) are gridded shield, power, and ground planes.

Aluminium wire bonds are made from the readout chips to the top trace layer only, and in the bond pad area a different gold ink (8 µm) is used. This is to provide for metallurgical compatibility with aluminium bonding wires and to achieve 100 µm track and gap resolution in these small dense areas. To allow discrete components to be soldered to the substrate, solder pads are printed with a silver/palladium ink. Finally, an insulator layer is printed over the whole circuit with openings at bond pad and solder pad sites.

Table 11-23 Forward module specification

Detector outer dimension	**Outer: 56.5 - 71.8 mm x 123.1 mm** **Middle: 56.1 - 75.3 mm x 118.7 mm** **Inner: 43.8 - 55.8 mm x 73.9 mm**
Construction	Use four *n*-on-*n* single sided detectors to form back-to-back glued detectors (two detectors back-to-back in the inner ring)
Mechanical tolerance	back-to-back: <5 μm (ϕ), <20 μm(z), <25 μm (r) Fixation point: <50 μm (ϕ), <100 μm (r)
Strip length	Outer: 121.1 mm (2 mm dead near the middle) Middle: 116.7 mm (2 mm dead near the middle) Inner: 71.9 mm
Strip directions	Fan (along r-coordinate), U/V (40 mrad stereo)
Number of readout strips	768/side, 1536/total
Strip pitch	Outer: 70.8 - 90.3μm, Middle: 70.3 - 94.8 μm, Inner: 54.4 - 69.5 μm
Hybrid	76 mm x 52 mm x 0.5 mm one double-sided hybrid, set at the end of the module
Detector power consumption	1 W/total @ 0°C, (Heat flux/300 μm) ~ 70 μW/mm^2
Hybrid power consumption	4.45 W
Operating temp. of detector	-7°C (average)
Uniformity of silicon temp.	<5°C
Permanent deformation	<5 μm (after 10 thermal cycles between -20 and +70°C)
Power on-off (Detector & Hybrid)	<10 μm
Dynamical deformation	<50 μm (between -10 and +30°C)

11.5.3.2 The forward module

Figure 11-55 is a schematic of the forward middle ring module showing the key features in the design. Figure 11-56 is an expanded view of the forward module. The two measuring planes, each formed of a pair of wafers as described in Section 11.5.2.1, are sandwiched around a double sided readout hybrid and a central spine. The spine serves as a mechanical support for the wafers and increases the thermal conductivity along the length of the module. The same double sided hybrid is used for all modules and is formed on a support board into which two slots have been made. The slots act as a thermal break to prevent heat from the front-end electronics from entering into the silicon wafers. The electrical connections from the silicon strips to the readout electronics are made via fan-in structures mounted on either side of the hybrid bridging the thermal break.

The front-end electronics chip-sets are separated into two groups by the primary cooling contact which also serves as the module mounting point. Additional cooling may be provided by a contact to the far end of the spine. The additional cooling contact is used only for full length middle ring modules.

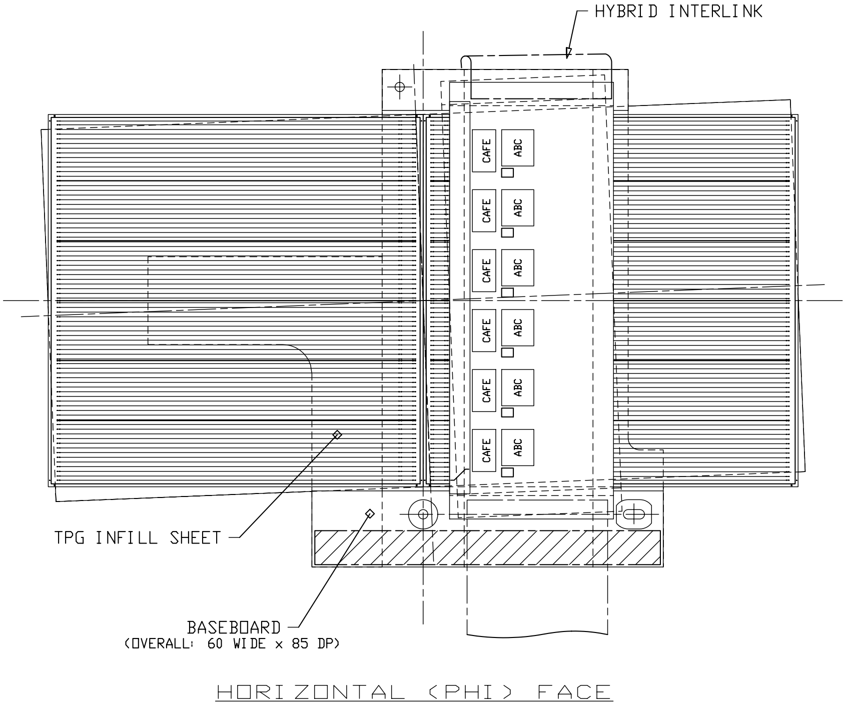

Figure 11-52 Configuration of the barrel module.

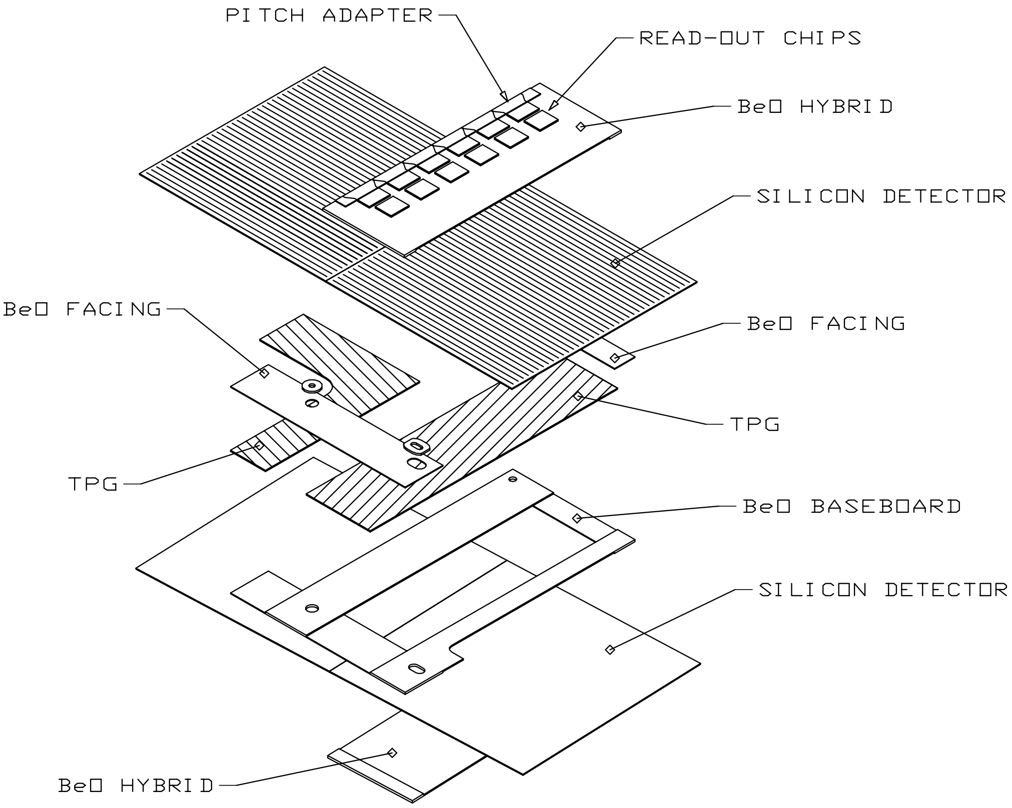

Figure 11-53 Expanded view of barrel module.

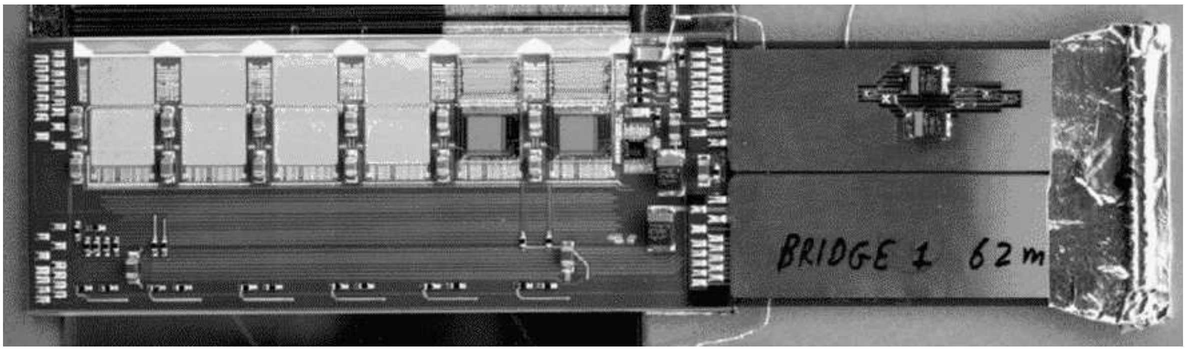

Figure 11-54 Photograph of barrel hybrid prototype.

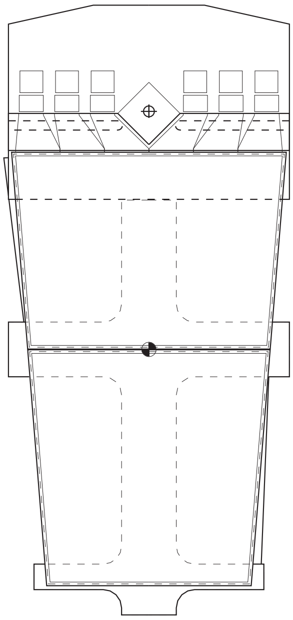

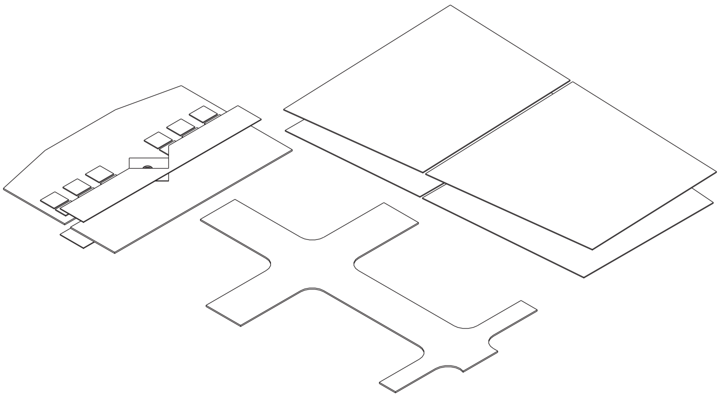

Figure 11-55 Forward module layout.

Figure 11-56 Expanded view of a forward module.

Figure 11-56 shows the details of the component parts for one of the three forward modules. All three designs are similar except for geometry dependent details. In the case of the outer ring, the electronics is mounted in-board the silicon to maximize the radial coverage allowed within the SCT geometry envelope. Furthermore the secondary cooling point, at the outer radius, is not required since the power dissipated in the silicon is much reduced due to the lower radiation dose. The inner ring, having an active length of 72 mm, does not require a secondary cooling contact.

Beryllia has been chosen for the hybrid base board and the spine due to its high thermal conductivity and long radiation length. The fan-ins are formed on glass with a low thermal conductivity.

A forward hybrid is shown in Figure 11-57. It is a double sided, multilayer thick-film circuit, fabricated on a 500 μm thick, laser profiled, beryllium oxide ceramic substrate. Prototypes have been produced using a thick-film screen printing process specially developed for this applica-

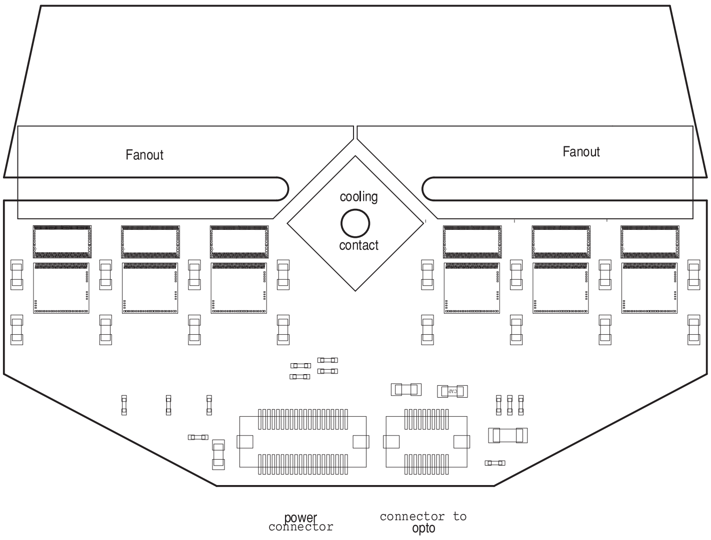

Figure 11-57 Layout of one side of a forward module hybrid.

tion. This, together with the use of 50% gridded power planes reduces the total radiation length in the metal layers by a factor of four as compared to standard thick film processes.

Each forward hybrid will have 6 sets of CAFE-M and ABC readout chip pairs, mounted and aluminium wire bonded on each side of the hybrid, together with a small number of passive decoupling components and connectors which are attached by soldering. The substrate has a number of small holes for through printed vias to provide for electrical connections between the two sides. The maximum dimensions are approximately 76 mm x 52 mm.

The hybrid circuit has four 3 μm thick screen printed gold interconnect layers on each side, with screen printed 200 μm vias and insulator layers (2*20 μm) between each interconnect layer. Connections between the two sides of the substrate are made by printed (gold filled) 180 μm vias. The first two metal layers on each side (nearest the substrate) are gridded power and ground contact to the far end of the spine. The additional cooling contact is used only for full length middle ring modules.

Details of the wire bonding to the top trace layer are identical to those foreseen for the barrel module hybrid (see Section 11.5.3.1).

11.5.3.3 Glues

SCT modules with n+ in n strip readout with an initial p+ in n implanted backside will have no glue contact on the n+ top side. The interest focuses on the back to back construction with glue contact between baseboard material and a passivated p+ implant surface. This side has an implanted guard ring structure which is specified to remain free from glue contact, but in other areas of the wafer thermal transfer of dissipated power must be made by the glue profiles, which could represent up to 10% of the wafer area. These areas of glue contact are in general somewhat larger than those needed in previous experimental assemblies.

There are two basic specifications needed for glues in the modules.These require that there is no deterioration in adhesive strength or increase in wafer stressing caused either (i) by temperature cycling from around -15°C to +30°C, or (ii) by subjecting them to integrated radiation fluxes up to 10^{14} low energy neutron/cm^2 equivalent. In satisfying (i) the module maintains a well-defined structural geometry, and the characteristics of achieving (ii) will be manifested by stable detector leakage currents during and after such irradiations. Results from Delphi and OPAL, with un-processed *p*-side contacts suggest no problem with various araldite based glues as well as Dow Corning Q1-9226. However only low levels of gamma radiation have been experienced by the LEP detectors. Some experience with araldite AW106/HV953 and Hexel 5313 Epolit resin/hardener exists for contacts with p+ in n surfaces indicating no increase in leakage for non-irradiated samples.

A systematic set of gluing tests has been carried out during a set of CERN PS irradiation studies. The measurements were aimed at studying both the chemical and mechanical effects of glue on the surface of devices, as well as the effects of proton irradiation on those devices for doses up to 2.2 x 10^{14} proton/cm^2. The basic test devices were 8 mm by 8 mm p+ in n diodes, 300 µm thick with a metallised deep *p*-implant area of 5.6 mm by 5.6 mm. All diodes had silicon dioxide capacitor dielectrics, which were produced through one of two different processing sequences. Some diodes were used as controls, and others were prepared and treated as follows: Silox passivated:

a) Two devices had glue 2011 applied above top passivation within the boundary of the metallised area, and a further two were treated in the same manner using glue 2019.

b) One sample of each type also had the glue across the guard rings. These devices were cured for twenty four hours at about 50^o C, and all showed no change in either bulk or guard currents.

c) Again glue 2011 was applied to one device as in (a) and to a further device as in (b)

d) The procedures of (c) were repeated with araldite on two further devices.

These were cured for twenty four hours in nitrogen at room temperature, and it was observed that diodes with only central glueing showed no ill-effects, but where glue was put across guard regions dramatic increases were seen in guard currents.

For such passivated structures it is concluded that glue over guard rings followed by slow cure at room temperature results in guard current increases, possibly due to depletion reaching the diode edge. This does not occur when a fast cure is made at high temperature and no effects are seen for glue applied to the central diode area.

In a study of unpassivated devices:

a) Two single-sided devices were treated with silver loaded epoxy on the *p*-side metallised implant, and then cured for twenty four hours at room temperature in nitrogen, with no observed deterioration of performance.

(b) Eight devices had glue 2011 applied to the *p*-side of the central diode, and again cured as in a), with no general deterioration observed, except two structures which showed slight increases in current, but only at voltages around 200 volts.

Seven unpassivated structures had ceramic discs glued with 2011 to the *p*-side of their central diode, and then cured for twenty four hours at room temperature in nitrogen. All devices showed dramatic increases in current, although it must be noted that before curing all currents were stable and unchanged. When repeated with four silox passivated devices this procedure resulted in no ill-effects, even after curing. The same procedures were applied to two polyimide passivated devices, with one showing current increase after a slow cure, and the other being unaffected.

Some conclusions can be drawn from these studies:

a) Glueing across guard rings should be avoided, although a fast cure may be helpful.

b) Bare glue (2011 and silver loaded epoxy) cause no ill-effects even on unpassivated surfaces.

c) Glueing ceramic to unpassivated surfaces is not satisfactory, and could be a result of the curing process, but silox passivation appears to protect against these problems.

d) Polyimide passivation appears not to provide protection against effects for the glueing plus curing processes.

11.5.3.4 Irradiation of module materials

Radiation effects on kapton laminates were studied in a 12 GeV proton beam at KEK, with an integrated fluence of 2 x 10^{14} p/cm^2 uniformly distributed over a 6 cm x 5 cm area.

The samples had 4 copper layers of 8 µm thickness. Each was glued on a 25 µm kapton sheet with a 10-25 µm adhesive layer. Internal copper layers are glued with Epoxy nitric adhesive and the cover layer with Epoxy acrylic adhesive. The peel strength of the kapton base layer and cover layer against a corresponding adhesive layer was measured. For the cover layer, for instance, these were 0.52 N/mm and 0.56 N/mm for before and after the irradiation respectively. The measurements show no deterioration, rather the peel strength increased slightly after irradiation.

The bonding pad adhesion was also examined by pulling out bonding wires which were bonded before the irradiation. The bonding wire is 25 µm diameter aluminium, and the bonding pad is gold-plated copper with a nickel intermediate layer. The force to break the bond did not change after the irradiation, and no damage on the bonding pad was observed after pulling off the wires of the irradiated samples. The irradiated samples were examined with a microscope, and no visual defects nor colour change were observed.

11.5.4 Module Performance

The module designs for both barrel and forward regions are at an advanced stage following extensive studies, both in simulation and prototyping of all vital features: electrical performance, mechanical structure and thermal management.

The concepts of current modules embody much information gained from a programme that has spanned a range of separate investigations. These have included studies of basic design components through to the construction of both partial and complete working modules. This section provides an overview of the most important contributions and summarises the performance that will be achieved.

11.5.4.1 Electrical performance

As detailed in Section 11.4 the performance of the front-end electronics is well matched to the demands at the LHC of both high interaction rates and high levels of background radiation. The final CAFE-M and ABC chip set or ABCD chip will be used. All the prototyping used an earlier chip set consisting of the CAFE chip, fabricated by ATT, and the CDP. The CDP is a radiation hard binary pipeline designed to run at 40 MHz but without the full SCT readout protocol. In addition to the CAFE, some prototyping used also an earlier chip called the LBIC, a rad-soft bipolar front end fabricated by Tektronix. The LBIC is faster than required for the SCT and has higher noise. Nevertheless it is useful when making comparative measurements where the noise level factors out.

Prototype hybrids have been designed and manufactured for the CAFE-CDP chip set and fabricated in a thick film process on aluminium nitride. These have performed to the required specification in both noise and uniformity of multi-chip response, and have been built into prototype barrel modules, together with both CAFE and LBIC front end chips.

A small number of similar hybrids, again relevant to the CAFE-CDP chip set, have been designed specifically for the forward module prototypes. These use the gridded plane/thin gold process on BeO, described earlier, and have led to a successful beam test of a forward module.

A number of electrically functional modules have been constructed. Some of these were fully configured back-to-back modules while others were either single-sided or partially instrumented. Although none of these modules is identical in mechanical or electrical detail to the current design, each has made a contribution to the understanding of the module concept. A schematic illustration of a prototype barrel module under test is given in Figure 11-58. A photograph of a prototype barrel module is shown in Figure 11-59.

Barrel prototypes

Barrel modules prototypes were fabricated from 12 cm long n^+-in-n detector pairs with 75 μm strip pitch. Some results are summarized in Table 11-24 which show the improved noise performance of the centre-tapped configuration. In addition, no systematic variation of threshold was observed for chips mounted across a module.

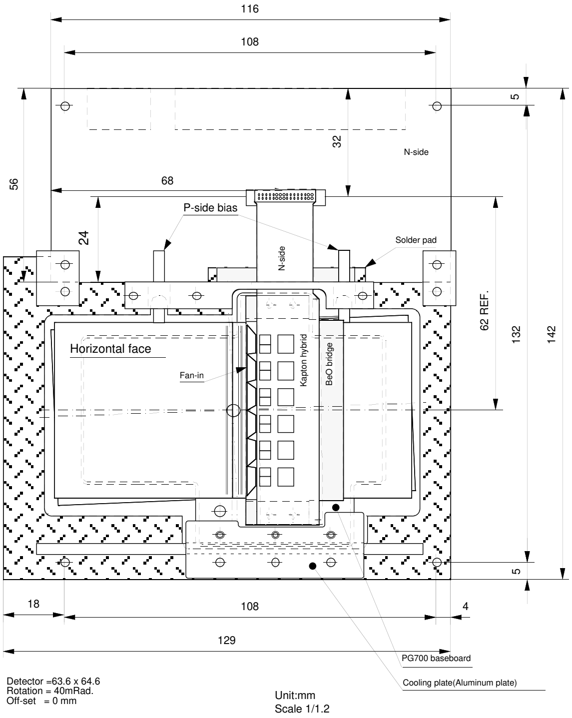

Figure 11-58 Prototype barrel module test arrangement.

A key aspect of the beam tests was to emulate actual ATLAS operating conditions. To this end, both irradiated and non-irradiated detectors were used in the beam test modules [11-69]. In addition, some operating parameters were chosen to simulate the conditions during ATLAS operations, with temperatures around -10°C and a magnetic field of 1.56 Tesla. In beam tests the efficiency was determined with the use of a high resolution silicon telescope and the noise performance of the detectors was characterized by the "off-track occupancy". This is defined to be the number of hits outside a 500 μm wide road around a track, divided by the total number of good strips in the wafer. The latter were estimated from measurements of the noise occupancy without beam.

The parameters that directly relate to the quality of track reconstruction for physics studies are the efficiency, noise occupancy and position resolution. Figure 11-60 shows the efficiency and noise occupancy as a function of threshold for a non-irradiated module. In this figure, 80 mV

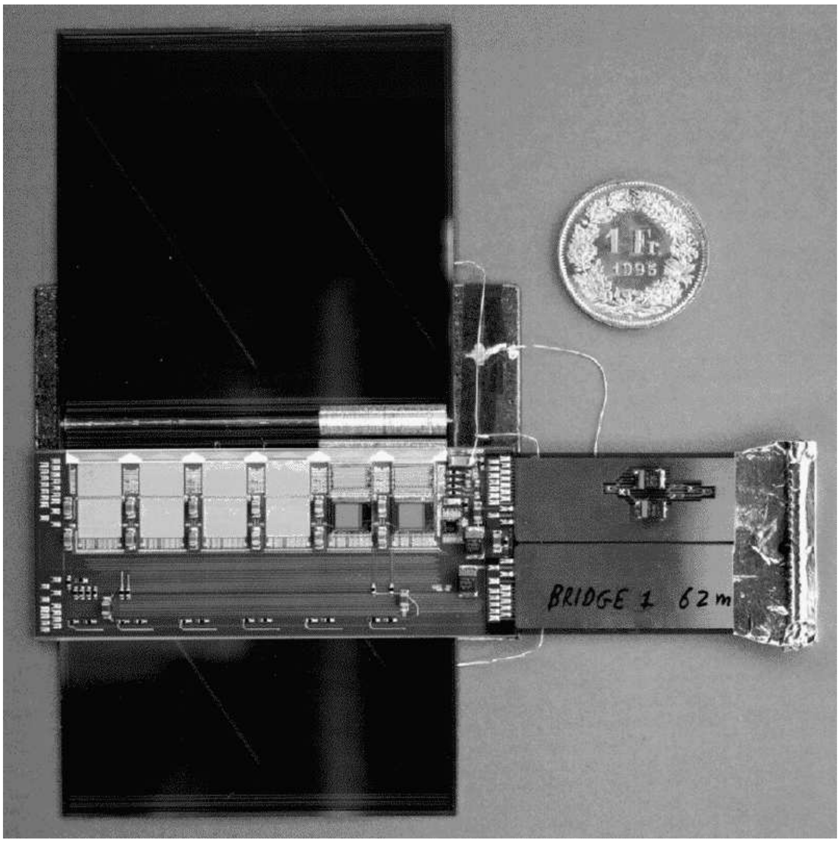

Figure 11-59 Barrel module electrical and test beam prototype. Material protruding from behind silicon is TPG heat spreader.

Table 11-24 Comparison of rms. noise and occupancy at 1fC discriminator threshold, for centre-tap and end-tap modules.

Barrel module	Wafer configuration	Readout configuration	RMS noise (electrons)	Occupancy at 1 fC threshold
EBP1	Back-to-back	Centre-tap LBIC+CDP	1830 e	6x10^{-4}
EBP2	Single-sided	Centre-tap CAFE+CDP	1300 e	<10^{-3}
EBP3	Back-to-back	End-tap LBIC+CDP	1970 e	17x10^{-4}

corresponds to 1 fC. Similar results were found for an irradiated module and are shown in Figure 11-61. In order to compare the occupancy with the ATLAS requirements, the numbers measured here should be divided by 2.5 to be normalized to the width, in clock cycles, of the CAFE comparator output pulse. The data thus confirm an expected performance of greater than 99% efficiency at a 1 fC threshold with an occupancy significantly better than 10^{-3}. Measurements were also made in a 1.56 Tesla magnetic field demonstrating good tracking efficiency over a wide range of module rotations (see Figure 11-62). These also showed that position resolution of ~20 μm was independent of rotation for thresholds greater than 1 fC (see Figure 11-63).

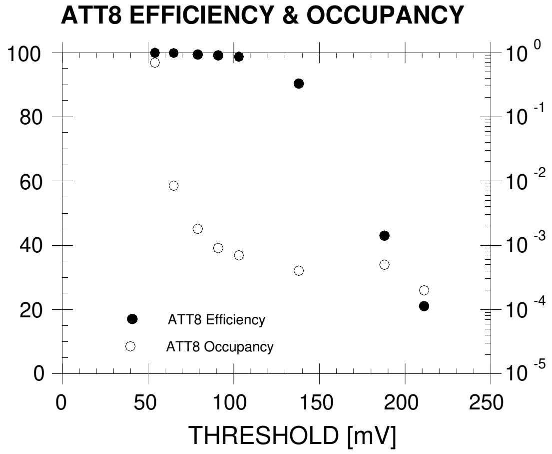

Figure 11-60 Efficiency and occupancy versus threshold for non-irradiated barrel module.

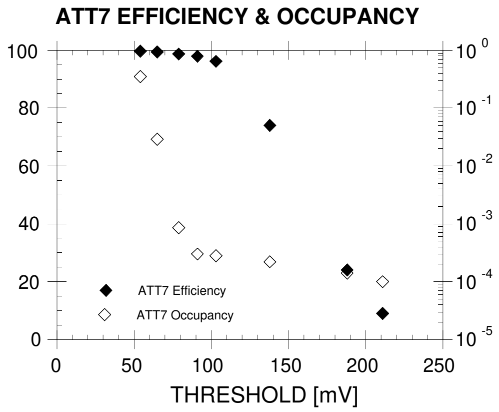

Figure 11-61 Efficiency and occupancy versus threshold for irradiated ($1 x 10^{14}$ p/cm^2) barrel module.

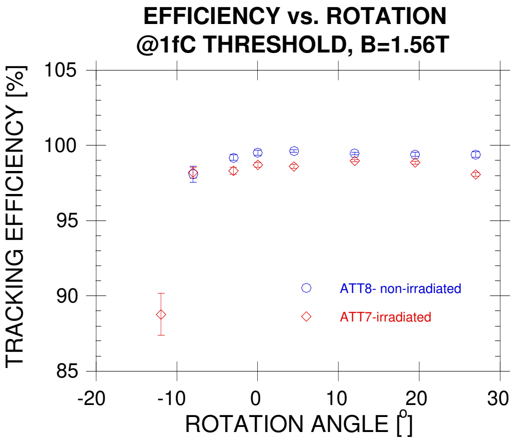

Figure 11-62 Efficiency versus angle for a 1 fC threshold.

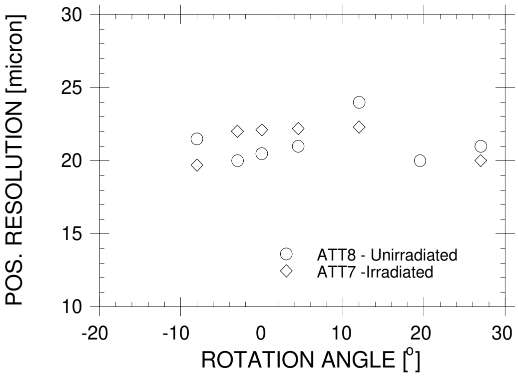

Figure 11-63 Position resolution versus angle for a 1 fC threshold.

In summary:

- Non-irradiated detectors, operated over-depleted at 175 volts with a binary threshold of 1 fC showed efficiency in excess of 99%. Detectors irradiated to a fluence of 10^{14} p/cm^2 and operated at 275 volts (full depletion was at 300 volts), with a binary threshold of 1 fC, showed efficiency in excess of 97%. The same device, operated at 150 volts was still 95% efficient.
- At a binary threshold of 1 fC, both irradiated and non-irradiated modules showed noise occupancies $<5 \times 10^{-4}$ and good efficiency and spatial resolution, over a wide range of rotation angles when in a high magnetic field.

Additional details are given in reference [11-69].

Forward prototypes

Forward prototype modules have also been constructed with single and double length wafer configurations. A photograph of one such module is shown in Figure 11-64. Figure 11-65 shows the noise values in the laboratory obtained by fitting error functions to the efficiency versus threshold curves and correcting for the absolute calibration for a range of charge magnitude injected into the front-end calibration circuitry. With the module at 6.5 cm strip-length a horizontal straight-line fit to the data yields an equivalent noise charge of 1112 rms electrons and at 12 cm the figure is 1513 rms electrons. In Figure 11-66 the noise occupancy as a function of threshold for the full-length module is plotted. At a threshold value corresponding to 4 times σ{noise} (=0.97 fC) the occupancy is approximately 10^{-4}.

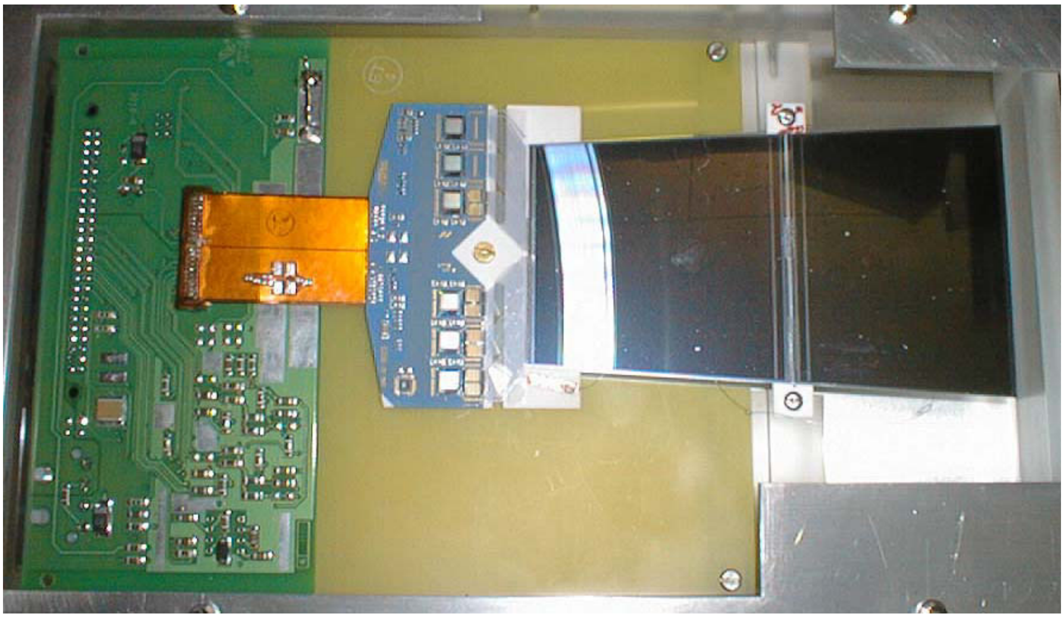

Figure 11-64 Forward module electrical and test beam prototype.

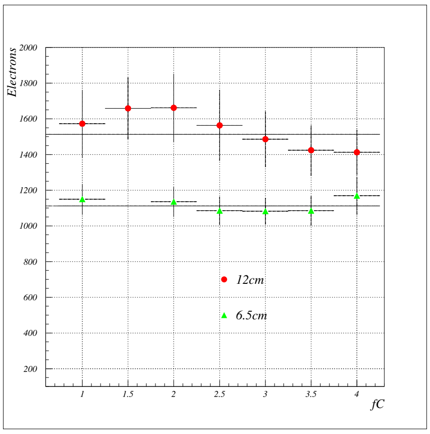

Figure 11-65 Forward module noise versus threshold for 6 and 12 cm strips.

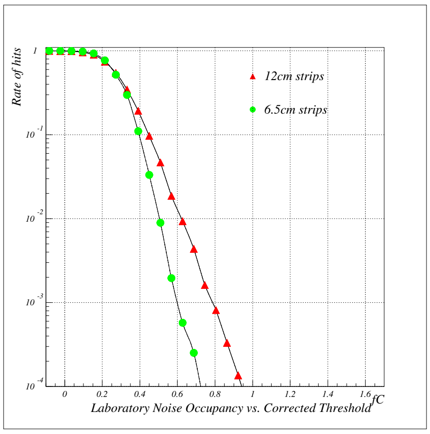

Figure 11-66 Forward module occupancy versus threshold for 6 and 12 cm strips.

A forward single-sided silicon module was tested in the CERN H8 test beam. Two separate wafer fabrications were required to form 12 cm strip-length modules, each wafer containing either a 6.5 cm-long, full-width narrow wedge-shaped detector or a 5.5 cm-long broader partner. The readout pitch varied from 70 µm at the narrow end to 90 µm at the broad end, the number of channels being 770. In operation the outer two channels would not be instrumented but would however be tied to the same potential as the others. In this way, readout strips with asymmetric electric field profiles at the detector edges are avoided. The detectors were fabricated from n bulk silicon with n+ strips.

The forward module was populated with six CAFE chips. Only two of the CAFE chips were full specification quality devices so only these two were bonded to the detector channels. The detector and hybrid were each glued to a flat rectangular piece of ceramic, avoiding the junction-side guard region, using slow-cure Araldite. No evidence of detector degradation in terms of its leakage current was observed post-gluing and bonding. The back-plane contact was achieved by means of connecting a fine wire to the large unpassivated region with conductive epoxy.

For every channel the pedestal offset relative to the mean of the distribution was recorded in a database. Test beam data were analysed and for each applied threshold plots of efficiency and noise occupancy versus corrected threshold were produced. Figure 11-67 shows the graphs which are obtained by combining the individual plots from the whole scan at 80V bias. In this case only 3 of the 128 channels are rejected and the efficiency is statistically consistent with 99% or above up to a threshold of 1.35 fC. The noise occupancy diminishes to a value of 10^{-3} at 0.7 fC threshold giving a 0.65 fC 'headroom' of operation. The long tail present in the occupancy plot is attributable to cases where a particle track has intersected the active region of the forward module but has missed the 3 x 3 cm sensitive window of each hodoscope plane (thus escaping the track multiplicity veto).

Track extrapolations to the forward module using the silicon telescope allowed resolutions to be measured. The r.m.s. values obtained are 20 µm and 14 µm for the single-strip and double-hit cases respectively and the track extrapolation error is insignificant at the 1 µm level when subtracted in quadrature. At this beam position the mean pitch was estimated to be 72 µm. The upper plot in Figure 11-68 shows the variation in resolution with threshold. For the data taken at 300 volts the resolution was measured to be 22 µm which is also in correspondence with pitch/ $\sqrt{12}$ at an approximate mean pitch of 78 µm.

One of the key issues with this detector design is the extent to which the deposited charge is divided between strips. With binary readout electronics the goal is to have all of the charge appearing on one strip only, as often as possible, in order that the efficiency is maximised. Concern was expressed that the accumulation electrons which reside in the gap between individual *p*-stops effectively mimic the presence of an extra *n*-type implant strip thus enhancing charge division by capacitive coupling. The ratio of single to double-channel clusters observed in Figure 11-68 shows that charge division is only occurring at an appreciable level in below 10% of cases at this threshold. In Figure 11-68 the proportion of double-channel clusters is plotted as a function of applied threshold. At 0.8 fC this proportion is around 11% and the figure falls with increasing threshold as the front-end comparator becomes less sensitive in the channel which collects the minor portion of the liberated charge.

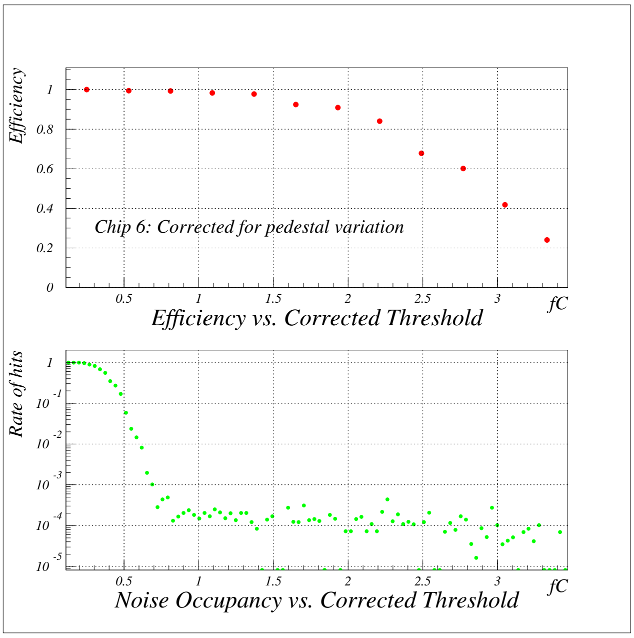

Figure 11-67 Forward module efficiency and occupancy versus threshold from beam test.

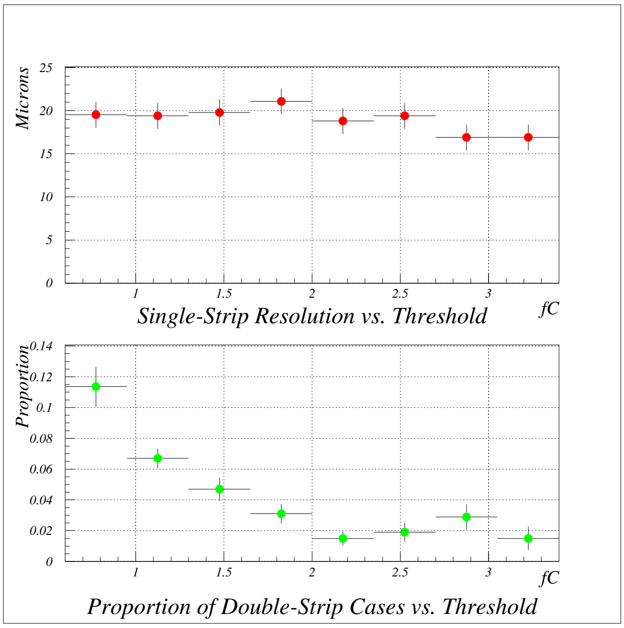

Figure 11-68 Forward module resolution and cluster length versus threshold.

11.5.4.2 Mechanical and thermal performance

To optimise module design a number of simulations have been done to understand the internal temperature distributions due to the heat dissipated by both the front end chips and the detector leakage currents. Thermal distortions have been calculated to be small, at the level of a few microns and have been confirmed by measurement for temperature variations over ~40° C range.

A critical issue is also the possibility of thermal run-away and finite element thermal simulations of the module designs have been made to study this.

Barrel modules

Studies of temperature distributions and thermo-mechanical effects on prototype barrel modules have been carried out by a number of groups within the SCT. In general this work involved dummy modules fabricated with electrically inert but thermally and mechanically correct materials. An example of such a device is shown in Figure 11-69. In this particular case, PG700 was used as a baseboard to provide very high thermal conductivity. A BeO ceramic plate was used as a dummy hybrid. An aluminium cooling pipe was attached to an extended lip of the base plate using a lubricant in order to achieve a good thermal contact between the base board and the aluminium pipe. Heaters were installed appropriately to simulate heat generation in the silicon detectors and front end readout chips.

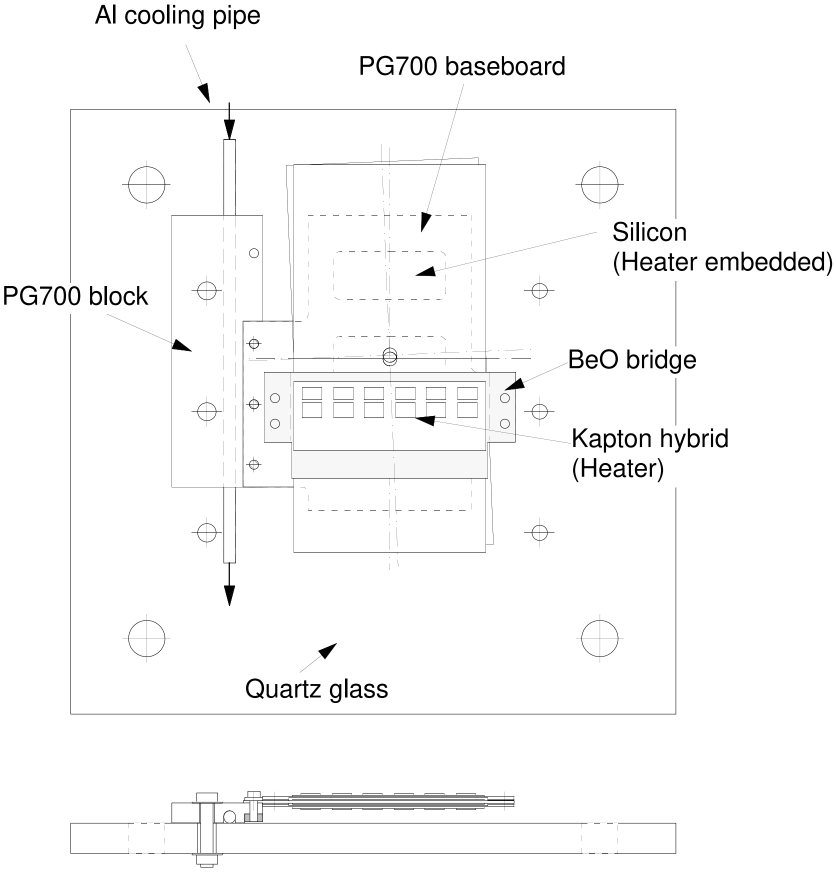

Figure 11-69 Dummy barrel module and mounting used for thermo-mechanical studies.

The test module was placed inside an environmental chamber. Both the ambient temperature inside the chamber and also the pressure were controlled in these measurements. The ambient temperatures was set to 0°C. The heaters were powered with 1 W for the silicon detectors and 3 W for the hybrid pair. The results are shown graphically in Figure 11-70. The data taken in vacuum were particularly useful in separating out the contribution of air convection cooling and to find parameters for use in finite element analyses. The observed results show temperature gradients across the module which are acceptable for use in the ATLAS SCT. These results are in good agreement with simulations and are confirmed in similar thermal modules also using PG heat spreaders, where the temperature difference between the coolant and the maximum hybrid temperature has been measured to be as low as 5.4°C [11-70].

Temprature profile of thermal modules
in 1atm. and a vacuum

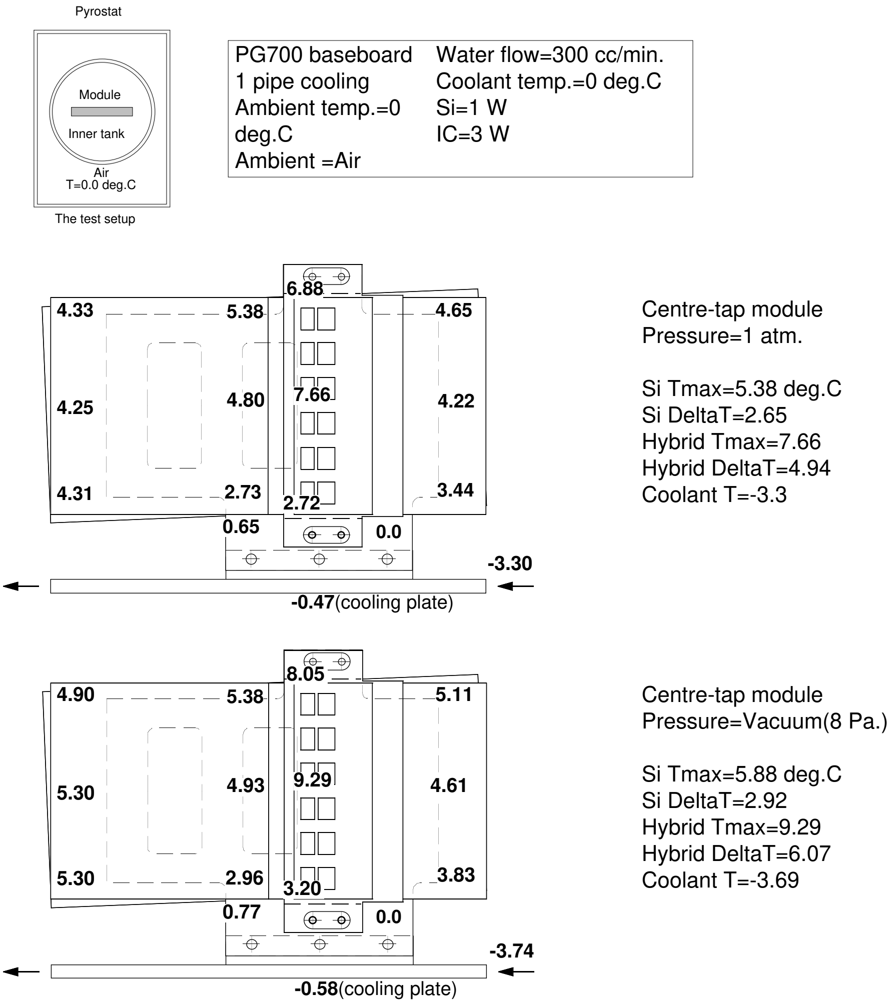

PG700 baseboard
1 pipe cooling
Ambient temp.=0 deg.C
Ambient =Air

Water flow=300 cc/min.
Coolant temp.=0 deg.C
Si=1 W
IC=3 W

Centre-tap module
Pressure=1 atm.

Si Tmax=5.38 deg.C
Si DeltaT=2.65
Hybrid Tmax=7.66
Hybrid DeltaT=4.94
Coolant T=-3.3

Centre-tap module
Pressure=Vacuum(8 Pa.)

Si Tmax=5.88 deg.C
Si DeltaT=2.92
Hybrid Tmax=9.29
Hybrid DeltaT=6.07
Coolant T=-3.69

Figure 11-70 Measured temperature distribution on test module containing PG heat spreader.

Figure 11-71 shows the thermal profile of a similar test module constructed without a PG insert, using only beryllia as a thermal baseboard, with a conductivity almost three times less. The larger temperature gradients are observed.

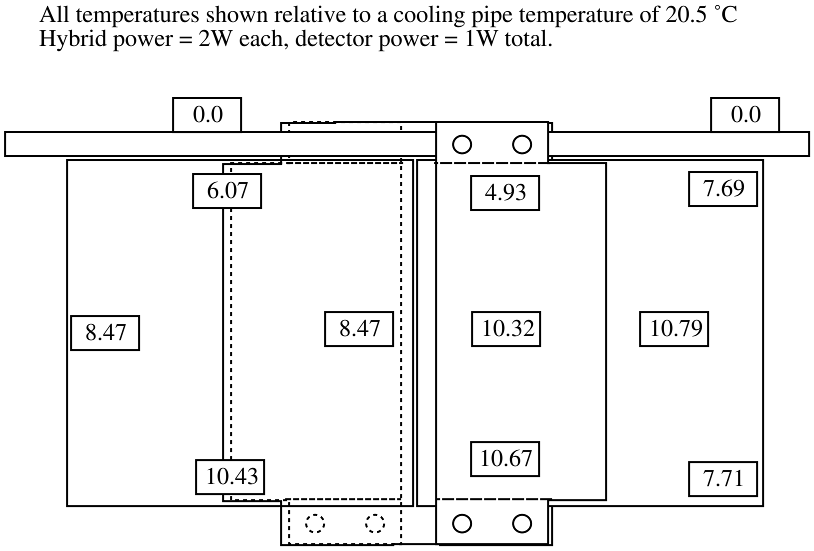
All temperatures shown relative to a cooling pipe temperature of 20.5 ˚C
Hybrid power = 2W each, detector power = 1W total.

Figure 11-71 Measured temperature distribution on barrel module without PG heat spreader.

The process of thermal runaway has been demonstrated to take place in radiation damaged silicon detectors [11-71]. A silicon strip module was fabricated using two irradiated detectors. A mock hybrid, instrumented with a 3 W heater was placed near the middle of the module. A cooling pipe ran over the edge of the hybrid and the temperature of the furthest corner of the silicon was measured as a function of the bias voltage applied to the irradiated detectors. Heat was therefore generated in both the silicon and the hybrid. In this particular study stable thermal containment was obtained for all relevant bias voltages for cooling/air temperatures below 10° C, and runaway actually occurred at 250 V bias when they were increased to 20° C [11-71].

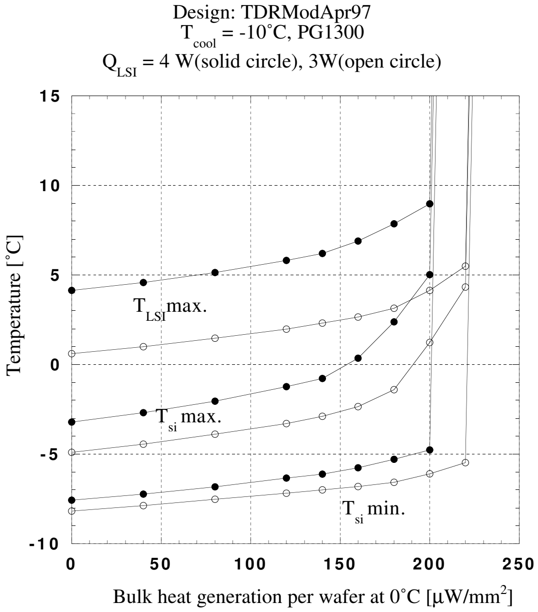

Figure 11-72 Results of thermal run-away simulation for the SCT barrel module.

For the final barrel module design (see Figure 11-52) a thermal simulation was done. Figure 11-72 shows the maximum (T_{si} max) and the minimum (T_{si}min) temperature of the silicon detectors in the module as a function of the bulk heat generation normalized at 0˚C, together with the maximum temperature of the readout chips (T_{LSI} max) from this simulation. The curves with the open circles are for a total front end chip power dissipation of 3 W and the closed circles for 4 W. This simulation shows that the thermal runaway of the silicon detector occurs at 200 µW/mm^2 for the 4 W chip power. The bulk heat generation after 10 years of operation at LHC is estimated to be 70 µW/mm^2 in the worst case. The barrel silicon strip module, thus, has a worst case safety margin factor of three.

Another important thermo-mechanical issue concerns distortions between the construction temperature of ~25°C and the operating temperature of ~ -10°C. The thermal test barrel module (see Figure 11-69) was measured using an ESPI system which is sensitive to distortions of 250 nm or larger. The module was mounted on a PG700 block which was rigidly attached on a pyrex glass plate of very small CTE and placed inside an environmental chamber to control the module and ambient temperatures. The distortion appeared as a fringe pattern of the ESPI measurement. This measurement was particularly sensitive to displacement near the perpendicular direction with respect to the module surface. The distortion was measured as the module was cooled down gradually from 24°C to 0°C. This is shown in Figure 11-73.

Figure 11-73 Barrel module distortion versus temperature.

The measured distortion of the module was 9 μm when cooled from 24°C to 0°C without turning on the heaters. When heaters were turned on with 1 W for the silicon and 3 W for the chips the incremental distortion was 4.8 μm at 0°C and 1 μm at room temperature. The results are shown in Figure 11-74 and Figure 11-75.

Figure 11-74 Barrel module distortion versus hybrid power at room temperature.

Figure 11-75 Barrel module distortion versus hybrid power near operating temperature.

Forward modules

Thermal modules corresponding to the geometry of the centre forward ring also have been constructed and tested. They used components fabricated from the correct materials (silicon and beryllia) or close substitutes (machinable glass ceramic instead of glass for the fan-ins). The hybrid and silicon heat loads were simulated using resistive wires attached to the components and thermocouples were used for temperature measurement. The measurements were performed at room temperature (22°C) with the temperature of the cooling fluid adjusted such that the ambient temperature was between the highest and lowest temperatures observed on the silicon. This procedure reduces the effects of non conduction (i.e. convection and radiation) heat losses on the measurements.

Adobe’s PostScript Language Reference Manual, 2nd Edition, section H.2.4
says your EPS file is not valid, as it calls setpagedevice

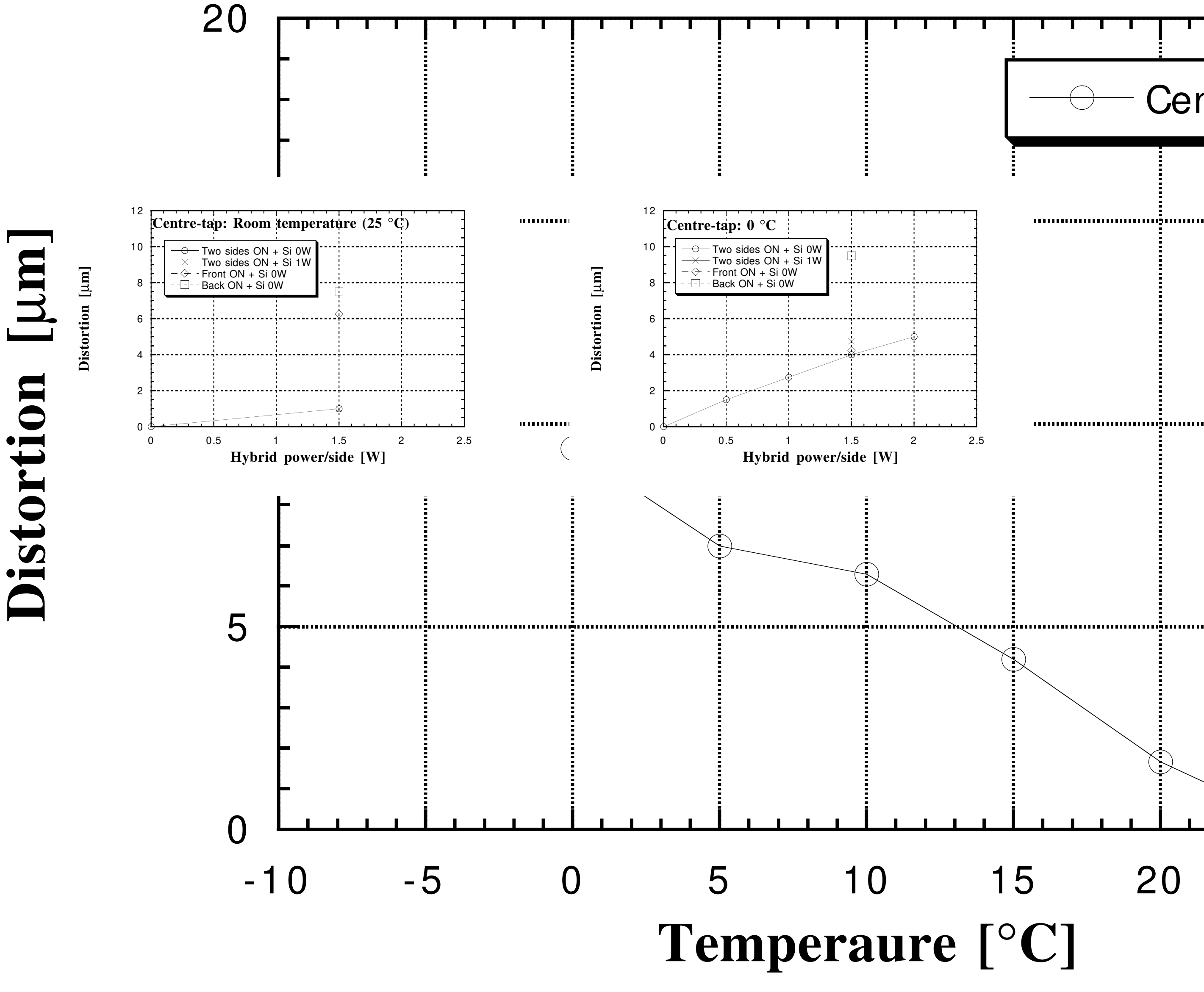
20
5
0
-10
-5
0
5
10
15
20
Distortion [µm]
Temperaure [°C]
Cen
Centre-tap: Room temperature (25 °C)
Two sides ON + Si 0W
Two sides ON + Si 1W
Front ON + Si 0W
Back ON + Si 0W
Distortion [µm]
Hybrid power/side [W]
0
2
4
6
8
10
12
0
0.5
1
1.5
2
2.5
Centre-tap: 0 °C
Two sides ON + Si 0W
Two sides ON + Si 1W
Front ON + Si 0W
Back ON + Si 0W
Distortion [µm]
Hybrid power/side [W]
0
2
4
6
8
10
12
0
0.5
1
1.5
2
2.5

The module was mounted on a board upon which two cooling blocks were mounted in the configuration corresponding to that of the middle and outer ring. The module was rigidly attached to the cooling block at the hybrid end and was simply resting on the block at the far end. The cooling path from the far end of the module, passing through the board to the inner ring cooling block, was designed to take out half of the power dissipated in the silicon.

Figure 11-76 shows the temperature measured at several points on the module. The measurement was performed in ambient air at 23.1°C with 3 W dissipated on the hybrid and 1 W in the silicon. The temperature of the coolant was adjusted so that the average temperature of the silicon was at ambient. In this configuration the coolant temperature was 17.5°C. The figure on the left shows the temperatures plotted as a rise above that of the coolant whilst that on the left shows the temperatures plotted relative to that at the module mounting point on the hybrid i.e. 3.6°C. The data show that the temperature of the silicon rises to 3.2°C above that of the module minimum at the mid-point of the silicon, with the temperature difference across the silicon of 1.6°C, and the temperature on the hybrid rising by about 9°C relative to the module minimum. The observations are in satisfactory agreement with the relevant simulation predictions.

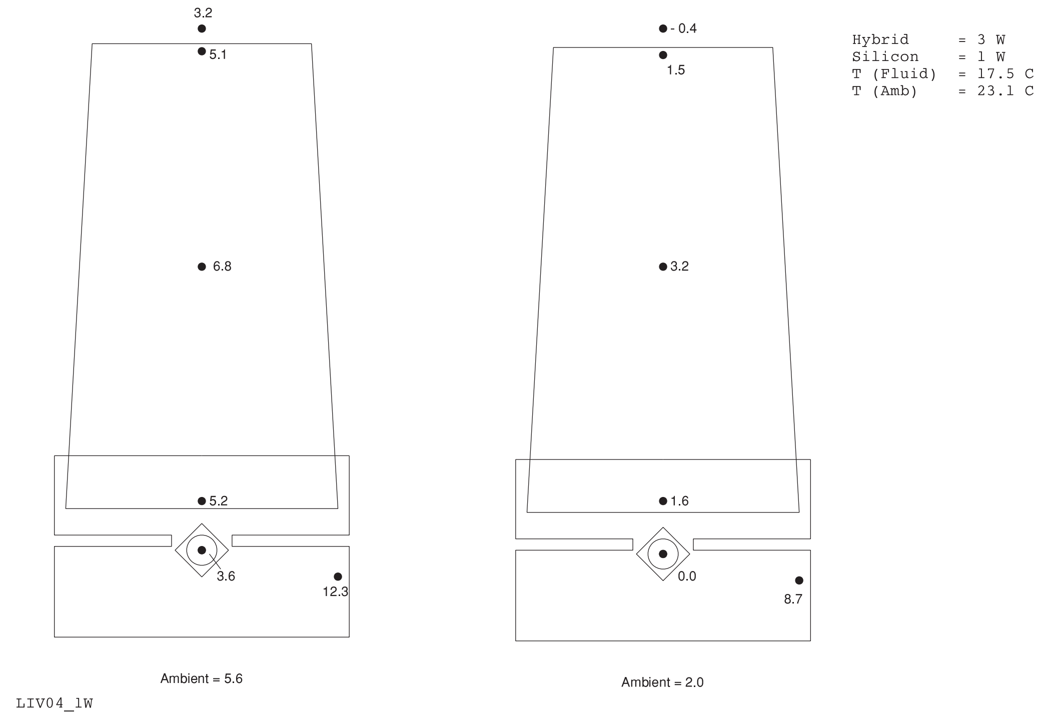

Figure 11-76 Temperature distributions on forward thermal test modules.

Thermal modules have also been subjected to temperature cycling across the temperature range -10°C to +20°C, to study mechanical distortions using an ESPI system. Maximum deflections, with the ambient temperature maintained at 0°C, were 30 μm for a module with a single-point cooling contact, and 3 μm when two cooling contacts were used. Studies of thermal runaway have also been made, with the conclusions that detector powers of 0.5 W and 2.0 W respectively could be satisfactorily contained for single-point and two-point systems respectively. Further optimization, with the possibility of including PG heat spreaders, could allow both cooling design options to be pursued into designs that would meet the needs of 10 year operation at LHC.

11.5.5 Component List and Materials

Module components

Table 11-25 lists the barrel module components, their numbers and critical dimensions. In some cases, most notably beryllia (BeO) items, the sizes given are the maximum length and width. Cut-outs, mounting holes or slots will reduce the effective dimensions. Quoted volumes are correct. The exact dimensions of the electrical components on the two, single sided hybrids are not given as final selection is not yet complete. Table 11-26 corresponds to the components for a full length middle ring forward module. In the case of the inner ring 6 cm long modules, the number of silicon detectors is reduced from four to two.

Table 11-27 shows typical values of the important thermo-mechanical and electrical properties of some of the module component materials. Significant variations can be found in the properties of glass used in thick films, and in varieties of pyrolytic graphite.

Table 11-28 and Table 11-29 show barrel and forward module components respectively, their radiation lengths, and their radiation length contribution to the modules.

Generic components of modules are listed in Table 11-30.

When considering variations in module components it is vital to ensure that the constructed device is made with high yield, has stable and well-defined geometry, and shows robust electrical performance. The front end electronics and hybrid, coupled with the detailed electrical properties of the wafer will determine the significance of the digitizing precision through the achievable signal-to-noise ratio. The internal mechanical stability and alignment specifications will then limit the ultimate spatial precision that can be achieved for tracks to be used in physics studies. As indicated in Table 11-30 the typical module contribution is 1.24% X_o. Roughly 20% of the radiation length comes from mechanical items (b,d,e) and 80% from electrically active elements (a,c,f). Of the latter, 65% are fenced by the need for maximum ionization signal. Any future changes will effect 0.48% X_o due to refinements in the electrical and mechanical design of the modules with final readout chips etcetera. The current barrel module design with a material estimate of 1.2% X_o has minimized all possible component items.

Table 11-25 Barrel Module

Component	No.	Length (mm)	Width (mm)	Thickness (mm)
Silicon detectors	4	64	63.6	0.3
Silicon detectors thermal adhesive	2	30	58	0.075
FE amplifiers (e.g. CAFE)	12	4	7.2	0.35
FE amplifiers thermal adhesive	12	3.5	6	0.075
FE amplifiers (e.g. ABC)	12	5.5	6.2	0.35
FE amplifiers thermal adhesive	12	5	5	0.075
TPG baseboard (Left hand)	1	40	40	0.38
TPG baseboard (Right hand)	1	22	85	0.38
BeO baseboard	1	60	85	0.38
BeO cover stiffener (pipe)	1	60	13	0.25
BeO cover stiffener (far)	1	42	7	0.25
Baseboard thermal adhesive	1	58	18	0.075
Baseboard double PEEK insert	1	5	4	0.75
Baseboard single PEEK insert	1	4	3.83	0.75
Glass fan-in	2	3.5	67	0.25
Fan-ins tracks	2	3.5	67	0.001
Fan-in adhesive	2	2.5	65	0.075
Beryllia hybrid board	2	28	74.6	0.38
Beryllia hybrid steps	4	28	4	0.25
Beryllia hybrid step adhesive	4	25	3	0.075
Thick film Au planes	6	60	23	0.003
Thick film glass layers	10	60	23	0.035
Thick film Au tracking	4	60	23	0.003
Interconnect cable kapton	1	24	11	0.025
Interconnect cable copper (Grnd)	1	24	11	0.005
Interconnect cable copper (tracks)	1	24	11	0.005
Other hybrid components	41	2	2	1
Capacitor solder pads	38	1.3	1.1	0.15
Capacitor Ag/Pa pad layer	38	1.3	1.1	0.015
Resistor solder pads	44	0.5	0.7	0.15
Resistor Ag/Pa pad layer	44	0.5	0.7	0.015
Kapton solder pads	100	1	1	0.15

Table 11-26 Forward Module

Component	No.	Length (mm)	Width (mm)	Area (mm^2)	Thickness (mm)
Silicon detectors	4	59.442	65.64	3901.77	0.3
Silicon detectors thermal adhesive	2	see figure	see figure	2179.58	0.075
FE amplifiers (CAFE)	12	4	7.2	28.8	0.5
FE amplifiers thermal adhesive	12	3.5	6.5	22.75	0.075
FE pipelines (ABC)	12	5.5	6.2	34.1	0.5
FE pipeline thermal adhesive	12	5	5.5	27.5	0.075
BeO spine	1	see figure	see figure	2911.52	0.5
Glass fan-in	4	10.2	33.6	342.72	0.25
Fan-ins tracks	4	10.2	33.6	342.72	0.005
Fan-in glue	4	see figure	see figure	383.04	0.075
Beryllia hybrid board	1	53.1	77	3819.87	0.5
Thick film Au planes (40%)	4	29.6	77	911.68	0.003
Thick film glass layers	8	29.6	77	2279.2	0.045
Thick film Au tracking (30%)	4	29.6	77	683.76	0.003
Aluminium washer	1	10	10	100	1
Other hybrid components	50	2	2	4	1
Hybrid connectors	3	20	3	60	1

Table 11-27 Material properties

Material	Thermal conductivity (W/m/K)	Radiation length (cm)	Young's Modulus (GN/m^2)	Density (gm/cc)	Thermal expansion (ppm/K)	Dielectric Constant
Silicon	126	9.36	113	2.34	2.6	11.7
Beryllia (BeO)	280	14.4	350	2.86	8.7	7
Pyrolytic graphite (typical)	700	19	20	2.2	-1.0 (x,y) 25 (z)	-
Thermal adhesive (typical)	0.8	12	0.1	2.2	110	4.5
Kapton	0.23	28.4	2.5	1.42	45	3.4
Aluminium	201	8.9	70	2.7	23.5	-
Gold	316	0.335	78	19.3	14	-
Thick film glass (typical)		8.0	75	2.4	32	6

Table 11-28 Barrel module components, their radiation lengths and their radiation length contribution to the module

Item	Material	Volume (mm^3)	X_0 (mm)	Rad len (%)
Silicon detectors	Silicon	4884	93.6	0.641
Silicon detectors thermal adhesive	Modified Araldite 2011	134	250	0.007
FE amplifiers (e.g. CAFE)	Silicon	121	93.6	0.016
FE amplifiers thermal adhesive	Die attach adhesive	19	250	0.001
FE amplifiers (e.g. ABC)	Silicon	143	93.6	0.019
FE amplifiers thermal adhesive	Die attach adhesive	23	250	0.001
TPG baseboard (Left hand)	Pyrolytic graphite	401	190	0.026
TPG baseboard (Right hand)	Pyrolytic graphite	711	190	0.046
BeO baseboard	Beryllia	952	144	0.081
BeO cover stiffener (pipe)	Beryllia	189	144	0.016
BeO cover stiffener (far)	Beryllia	74	144	0.006
Baseboard thermal adhesive	Modified Araldite 2011	47	250	0.002
Baseboard double PEEK inserts	Polyether ether ketone	26	319	0.001
Glass fan-in	Glass	117	123	0.012
Fan-ins tracks	Aluminium	0.1	120	0.000
Fan-in adhesive	Modified Araldite 2011	24	250	0.001
Beryllia hybrid board	Beryllia	1587	144	0.135
Beryllia hybrid steps	Beryllia	112	144	0.010
Beryllia hybrid step adhesive	Modified Araldite 2011	23	250	0.001
Thick film Au planes	Gold	10	3.35	0.036
Thick film glass layers	Glass	435	80	0.067
Thick film Au tracking	Gold	3	3.35	0.012
Interconnect cable copper	Copper	2.3	14.3	0.002
Other hybrid components	Silicon/ceramic	164	78	0.026
Capacitor solder pads	Lead/Tin	8	9.12	0.011
Capacitor Ag/Pa pad layer	Silver/Palladium	0.8	8.26	0.001
Resistor solder pads	Lead/Tin	2.3	9.12	0.003
Resistor Ag/Pa pad layer	Silver/Palladium	0.2	8.26	0.000
Kapton solder pads	Lead/Tin	15	9.12	0.020
			Total	1.20%

Table 11-29 Forward module components, their radiation lengths and their radiation length contribution to the module.

Item	Material	Volume (mm^3)	X_0 (mm)	Rad len (%)
Silicon detectors	Silicon	4682.12	93.6	0.641
Silicon detectors thermal adhesive	Modified Araldite 2011	326.93	250	0.016
FE amplifiers (e.g. CAFE)	Silicon	172.8	93.6	0.023
FE amplifiers thermal adhesive	Die attach adhesive	20.47	250	0.001
FE amplifiers (e.g. ABC)	Silicon	204.6	93.6	0.028
FE amplifiers thermal adhesive	Die attach adhesive	24.75	250	0.001
BeO spine	Beryllia	1455.76	144	0.129
Glass fan-in	Glass	342.72	123	0.035
Fan-ins tracks	Aluminium	6.85	89	0
Fan-in glue	Araldite 2011	114.91	250	0.005
Beryllia hybrid board	Beryllia	1909.93	144	0.17
Thick film Au planes	3 μm Gold	10.94	3.35	0.041
Thick film glass layers	Glass	820.51	110	0.095
Thick film Au tracking	3 μm Gold	8.2	3.35	0.031
Aluminium washer	“Aluminium”	100	89	0.014
Other hybrid components	Silicon	200	93.6	0.027
Hybrid connectors	Plastic and Be/Cu	180	89	0.025
			Total	1.28

Table 11-30 Generic module components

Component	X_0 (%)
(a) Silicon wafers	0.64
(b) adhesives	0.04-0.06
(c) front end chips	0.04-0.05
(d) mechanical baseboard	0.12-0,15
(e) thermal baseboard	0.06-0.08
(f) hybrid, with bonds and electrical planes	0.30-0.32
Summed material	1.20-1.28

11.5.6 References

11-68 I. Kipnis, Noise Analysis due to Strip Resistance in the ATLAS SCT Silicon Strip Module, LBLN Note 39307, August 1996.

11-69 F. Albiol et al., Beam Test of the ATLAS Silicon Detector Module with Binary Readout in the CERN H8 Beam in 1996, Trans. IEEE N.S. Symp., Nov 3-8, 1996.

11-70 G. Barbier et al., Status Report on Module Cooling and Mechanics, ATLAS Note ATLAS-INDET-NO-166 (1997).

11-71 T. Kohriki et al., First Observation of Thermal Runaway in the Radiation Damaged Silicon Detector, IEEE Trans. Nucl. Sci. 43 (1996) 1200-1202.
T. Kondo et al., ATLAS presentation ATLAS-SCT-TR-021 (March 1996).